Future enhanced threshold effects of wildfire drivers could increase burned areas in northern mid- and high latitudes

Check for updates

Hang Zhao [1,2], Zhengxiang Zhang [1,3] ✉, Xin Wang [1,2], Shuo Zhen [1,2], Hongyan Zhang [1,3], Zhao-Jun Bu [1,3], Jianjun Zhao [1,2], Xiaoyi Guo [1,2], Kejiang Wei [1,2] & Long Dong [1,2]

Wildfires exhibit extensive nonlinear characteristics and threshold effects in response to environmental changes. However, how threshold effects affect wildfire responses and their future changes remains unclear. Here we identified thresholds where wildfire-driver relationships shift and estimated the impact of threshold effects on wildfire dynamics in the 21st century in northern mid- and high latitudes (>30°N). Wildfire-driver thresholds, coregulated by gradient differences in heat and moisture conditions, vegetation productivity, and human activities, effectively explain the spatial patterns and uneven responses of wildfires. Despite the dominance of temperature, precipitation, and socioeconomic status on wildfires, 30.70% of wildfire changes are attributed to their threshold effects, notably in boreal and temperate ecosystems. Climate change will enhance the threshold effects of wildfire drivers, leading to a 47.81 ± 3.08% increase in burned areas by 2030–2100 compared with 2001–2022. Our findings highlight that enhanced threshold effects of drivers promote future wildfire changes, posing challenges to fire suppression.

Comprehending the response of ecological properties to environmental changes and their linkages to climate change is crucial to reveal the global ecosystem's evolutionary process and future changes[1,2]. Nonlinear relationships and threshold effects are pervasive in ecological processes' response to external pressure[3]. Specifically, ecological properties are relatively insensitive to external changes until those changes reach their thresholds; once these thresholds are approached or crossed, small changes produce disproportionate impacts on ecological properties, even causing abrupt and irreversible regime shifts[2,4]. Nonlinear responses and threshold effects increase the uncertainty and unpredictability of ecological processes, challenging the assessment of ecosystem stability and adaptability to climate change[5,6].

Wildfire is a representative ecogeographic process governed by nonlinearity and threshold effects[3,4]. Thresholds act as switches that, once exceeded, trigger wildfire occurrences or ecological process shifts. Therefore, wildfires are considered the final result of multiple drivers working together to reach their thresholds[7,8]. Similarly, cross-scale thresholds determine the transition in fire size from smaller to larger scales (e.g., from local scale to regional scale) and serve as key properties for revealing changes in fire behavior and multiscale interactions during wildfire spread. Beyond these thresholds, cross-scale interactions and feedback emerge, accompanied by

changes in the dominant driver of spreading wildfires[9,10]. Ongoing global warming may drive changes in external factors that reach thresholds, triggering broader and more intense wildfires[11,12]. In this case, even minor variations in wildfire drivers would cause dramatic changes and intensify the extremity of wildfires. These perspectives indicate the universality of thresholds and threshold effects in wildfire responses and highlight the importance and urgency of understanding their impacts and mechanisms.

Previous works have revealed nonlinear wildfire response patterns and determined thresholds for dominant wildfire drivers, such as temperature, precipitation, and fire weather indices[13–15]. These thresholds help clarify critical conditions for wildfire occurrence or explain regional differences in fire regimes and response characteristics. However, most thresholds were determined for entire regions or at broad spatial scales, neglecting the spatial heterogeneity of the thresholds across sub-geographic units. This limits the applicability of thresholds in similar ecoregions or localized subregions and the ability to analyze wildfires under threshold relationships[16]. Moreover, although threshold relationships between individual drivers and wildfires have been clarified[17,18], how the thresholds (or threshold effects) of different drivers interact and how the interplays of wildfire drivers are coupled with their threshold effects to control wildfires remain unclear. This gap exists

[1]Key Laboratory of Geographical Processes and Ecological Security in Changbai Mountains, Ministry of Education, School of Geographical Sciences, Northeast Normal University, Changchun, 130024, China. [2]Urban Remote Sensing Application Innovation Center, School of Geographical Sciences, Northeast Normal University, Changchun, 130024, China. [3]State Environmental Protection Key Laboratory of Wetland Ecology and Vegetation Restoration, Institute for Peat and Mire Research, Northeast Normal University, Renmin 5268, Changchun, 130024, China. ✉e-mail: zhangzx040@nenu.edu.cn

because parameters for estimating threshold effects have not been integrated into frameworks and models to analyze multifactorial interactions, limiting the ability to capture nonlinear wildfire response characteristics in multi-factor settings.

Climate change may compel wildfire drivers to approach or surpass their thresholds over broader extents and amplify its impact on future wildfires by changing threshold effects[13,19]. Some studies warned that warming in the Arctic is reaching a threshold above which even minor warming could trigger an exponential increase in wildfires and a rapid shift in fire regimes[11,20]. However, the consequences of nonlinear changes in wildfires may be underestimated due to the inadequate quantification of threshold effects in current wildfire projection approaches[2]. For example, a lack of knowledge about threshold effects increases the uncertainty of future wildfire predictions, limiting the ability to explain the spatiotemporal variability in wildfires under climate change[4,18]. How wildfires respond to climate change under the influence of threshold effects and to what extent wildfire changes are related to threshold effects remain unclear. Thus, examining the role of threshold effects in wildfire changes is critical for accurately predicting future wildfire patterns and revealing the responses of wildfires to climate change.

Northern mid- and high latitudes (>30°N) are hotspots where wildfires exhibit the most substantial interannual variability and the most pronounced responses to climate change[21,22]. Here, the ecosystem stores more than 50% of global biological carbon and almost 30% of soil carbon[23,24], in which wildfires constitute the dominant ecological process controlling carbon emissions[25]. The feedback cycle shows that global warming is accelerating atmospheric and soil drying, thereby increasing the likelihood of more extensive and frequent wildfires[26]. Increasing wildfires due to warming climates in turn release additional CO_2, further contributing to global warming[25]. Therefore, clarifying wildfire dynamics in mid- and high latitudes under threshold relationships has global implications for understanding climate change, ecosystem functional shifts, and carbon cycles. This study aims to elucidate how threshold effects affect wildfire response processes and their future changes. We addressed three key questions: (a) What spatial patterns do the thresholds and threshold effects of wildfire drivers exhibit? (b) What key role do threshold effects play in wildfire driver interactions? (c) How will wildfires respond to climate change under the influence of threshold effects?

Results

Thresholds and threshold effects of wildfire drivers at ecoregional scales

We examined the relationships between burned areas (BA) and individual wildfire drivers in each ecoregion (Supplementary Figs. 1–7). The nonlinear response of wildfire to drivers was identified in 148 pairwise relationships (Supplementary Figs. 2, 4, 6), and valid thresholds were determined for 142 of these pairs (Supplementary Figs. 3, 5, 7). The impact of drivers on wildfires changed abruptly after thresholds were exceeded, in which threshold effects enhanced wildfire changes in 66 pairs of relationships but weakened wildfire changes in 76 pairs (Fig. 1).

Climate conditions in polar and boreal ecosystems were closer to their thresholds and had lower thresholds than those in other ecoregions (Fig. 1a–f). Thus, high-latitude climates, such as mean temperature (Tem_FS) and average monthly fire weather index (FWI_FS) during the fire season, were more likely to reach thresholds and trigger shifts in climate-fire relationships. In temperate ecosystems, total precipitation (Pre_FS) thresholds notably exceeded their regional averages (Fig. 1b). In contrast, thresholds for vapor pressure deficit (VPD_FS), preseason temperature (Tem_PFS), preseason precipitation (Pre_PFS), average leaf area index (LAI_FS), and gross domestic product (GDP) closely aligned with regional averages (Fig. 1d–g, i). Once these thresholds were exceeded, dry climates, increased vegetation productivity, and intensified human activities enhanced wildfire changes notably. This highlights that the threshold effects of moisture conditions, vegetation, and socioeconomic activities strongly influenced temperate wildfires. In most subtropical ecosystems, LAI_FS and total net primary production (NPP) are currently below thresholds and have

not yet reached a level where increasing vegetation productivity would weaken wildfire changes (Fig. 1g–h). In this case, dry climates, increasing human activities, and land cover change rate (LCC) until their thresholds were exceeded amplified wildfire changes (Fig. 1d–e, i, k). Conversely, regional averages of population (Pop) exceeded their thresholds by 1.5 orders of magnitude (~30 times), and population variation has somewhat weakened changes in subtropical wildfires (Fig. 1j). Overall, thresholds and threshold effects of wildfire drivers varied across ecoregions, but they were relatively consistent across ecoregions with identical climate zones.

Significant correlations and spatial covariation patterns were shown between thresholds of different wildfire drivers (Fig. 2). Positive correlations were found among the thresholds of Tem_FS, FWI_FS, VPD_FS, LCC, and Tem_PFS (Fig. 2a). These thresholds increased with increasing temperature across ecoregions, showing spatial patterns controlled by latitudinal differences in heat conditions (Fig. 2b; Supplementary Fig. 8). Positive correlations were also identified among thresholds for Pre_FS, Pre_PFS, LAI_FS, and NPP. These thresholds exhibited comparable spatial and latitudinal patterns that increased with elevated precipitation, vegetation productivity, and socioeconomic activity (Supplementary Fig. 8; Fig. 2b–d). Conversely, we found negative correlations among thresholds of FWI_FS, LAI_FS, and Pop, showing minimized FWI_FS thresholds in regions with high vegetation productivity and population thresholds. Such spatial patterns were controlled by gradient differences in temperature and vegetation productivity (Fig. 2b–d). However, positive correlations among the strengths of threshold effects were minimal and uncommon (Fig. 2a). Despite some similarities of variations in their threshold effects across spatial gradients (Fig. 2f–i; Supplementary Fig. 9), these drivers did not exhibit distinct spatial patterns in threshold effects. We only found that the threshold effects of GDP were correlated with those of LCC and enhanced with increasing precipitation (Fig. 2g).

Contribution of drivers and threshold effects on wildfires

The multifactorial model containing threshold parameters exhibited passable performance and robustness, with an explanatory power of 0.47 (Supplementary Fig. 10). Wildfire drivers and their threshold effects explained 69.30% and 30.70% of the BA changes, respectively, with a contribution ratio of approximately 7:3 (Fig. 3). Threshold effects had greater contributions to BA in subtropical steppes (33.05%) and deserts (30.37%), temperate steppes (34.90%) and deserts (34.40%), and boreal coniferous forests (30.45%), but lower contributions to BA in temperate coniferous forests (25.94%), subtropical humid and dry forests (27.13% and 17.93%), and boreal mountain systems (25.65%) (Figs. 3 and 4a, b). Accordingly, the contributions of threshold effects to the BA also exhibited a distinct spatial pattern along the latitudinal gradient. The threshold effects contributed most substantially (~30%) in the region between 47°N and 60°N, while the weakest contribution (~25%) was observed between 35°N and 42°N. In comparison, the remaining regions showed a contribution of approximately 27%. Overall, changes in wildfire drivers themselves dominated BA changes in northern mid- and high latitudes, and their threshold effects contributed to approximately one-third of the BA changes.

Precipitation (Pre_FS and Pre_PFS), GDP, FWI_FS, and temperature (Tem_FS and Tem_PFS) are the dominant wildfire drivers (Fig. 3). Precipitation explained 25.28% of the BA changes and served as the strongest explanatory variable of wildfires in 23.26% of the land areas (Supplementary Table 2), including deserts, steppes, and mountain systems in temperate and subtropical regions (Fig. 4c). The GDP explained 13.07% of the BA changes, notably affecting wildfires in 13.03% of the land areas, especially around human settlements. In contrast, temperature and FWI_FS explained only 8.82% and 6.21% of the BA changes during the fire season, respectively. They were the strongest explanatory variable of wildfires in 2.24% and 1.24% of the land areas, respectively, mainly in the mountain systems of eastern Siberia and North America and the temperate coniferous forests of East Asia. Moreover, the threshold effects of precipitation, temperature, LCC, and LAI_FS collectively explained 19.87% of the BA changes (Figs. 3 and 4d). They were the strongest explanatory variables of wildfires in 23.68% of
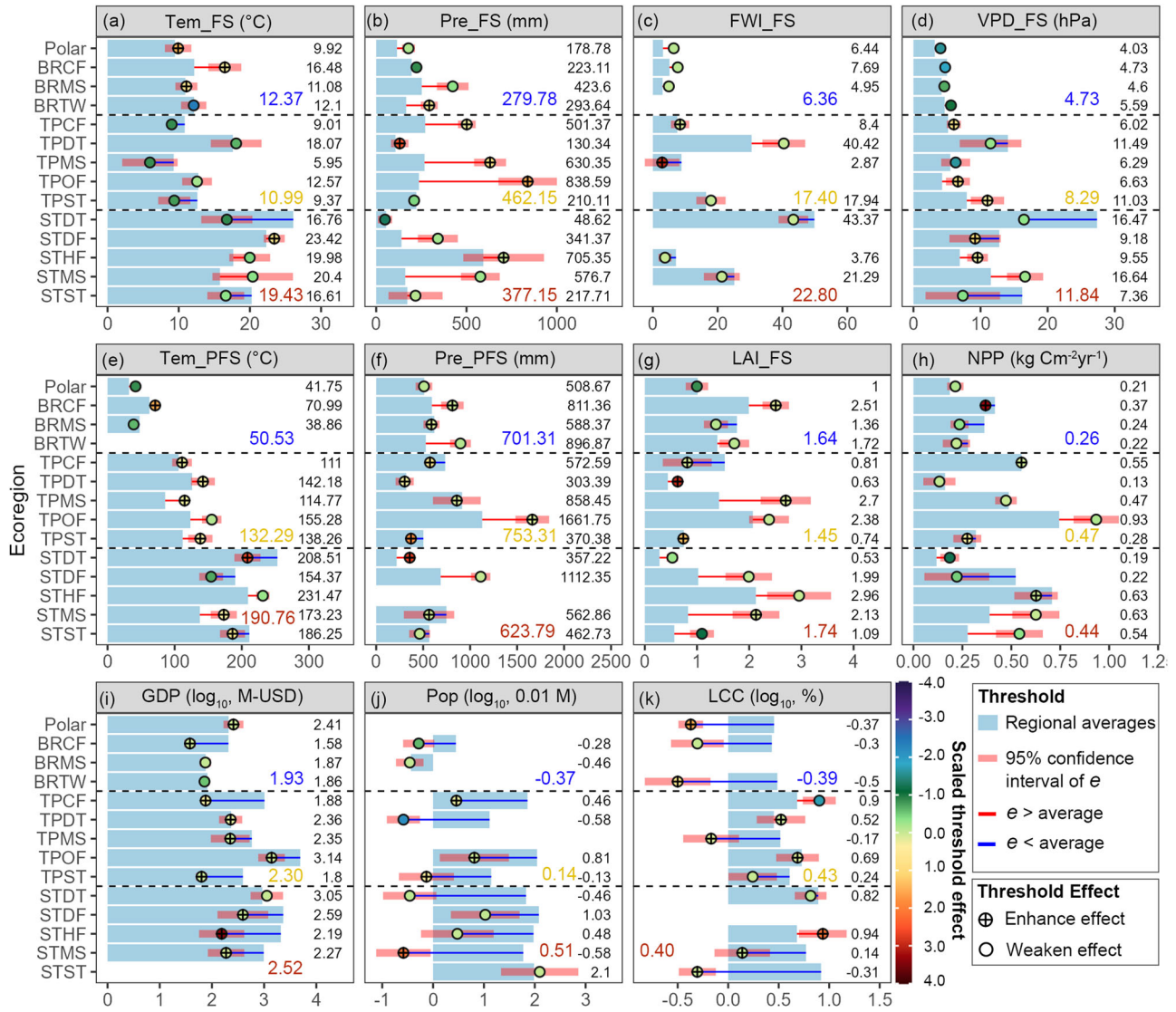
Fig. 1 | Thresholds and threshold effects of wildfire drivers at ecoregion scales. a–d Thresholds and threshold effects for climatic variables during the fire season: Tem_FS, Pre_FS, FWI_FS, and VPD_FS, respectively. **e–h** Thresholds and threshold effects for preseason climatic and vegetation productivity variables: Tem_PFS, Pre_PFS, LAI_FS, and NPP, respectively. **i–k** Thresholds and threshold effects for socioeconomic and anthropogenic variables: Pop, GDP, and LCC, respectively. Ecoregion abbreviations were defined in the Methods section. The blue bars are the average of wildfire drivers in each ecoregion, facilitating comparisons with thresholds. The positions of colored dots on the x-axis are the thresholds of wildfire drivers, with text labels on the right side. The color scale of the dots is the strength and direction of the threshold effects (z-score scaled). The blue, yellow, and red fonts are the average thresholds in the polar and boreal, temperate, and subtropical ecoregions, respectively. Note: The original values of Pop and LCC include decimals, resulting in negative values after logarithmic transformation. Supplementary Note 1 contains detailed information on the identification of threshold effects.

land areas when excluding the main contribution of the drivers and focusing only on threshold effects. The threshold effects of precipitation contributed more to wildfires than those of temperature (8.26% > 5.43%) and covered broader areas than the threshold effects of temperature (13.77% > 8.64%). Notably, wildfires in the tundra, woodland, and mountain systems in boreal ecosystems and temperate steppes were mostly controlled by threshold effects of temperature and precipitation. In summary, precipitation, temperature, and their threshold effects, alongside socioeconomic status, were the dominant factors that influenced wildfires over a vast spatial extent.

Future changes in wildfires under the impacts of threshold effects

Our model predicted the annual average BA during the fire seasons for each period in each of the four socio-climatic scenarios (Fig. 5). Their average showed that the BA in mid- and high latitudes will increase by 0.31 million km² from 2030–2100, an increase of 47.81 ± 3.08% compared with the

2001–2022 average. The rates of BA changes will decrease from 45.84% and 48.90% in the near term (2030–2050) to 41.53% and 46.13% by the end of the 21st century under the SSP1-2.6 and SSP2-4.5 scenarios, respectively. Conversely, the BA change rates will increase from 45.62% and 46.06% in the near term to 57.86% and 56.35% by the end of the 21st century under the SSP3−7.0 and SSP5-8.5 scenarios, respectively.

Future changes in BA during the fire seasons exhibited similar spatial patterns under four socio-climatic scenarios (Fig. 5a–f; Supplementary Fig. 11). By the end of the 21st century, 32.74% of the land surface will experience a large increase in BA (> 15 km² grid⁻¹). A notable decrease in BA (> 20 km² grid⁻¹) will emerge across 7.60% of the land surface. Notably, future BA changes are pronounced in temperate and boreal ecosystems across all scenarios (Fig. 5g–i). The promoting effects of higher emission scenarios on BA were accumulated in high latitude ecosystems with ongoing climate change, intensifying spatial differences in BA changes across scenarios (Fig. 5a–f; Supplementary Fig. 11). Statistics also revealed that BA
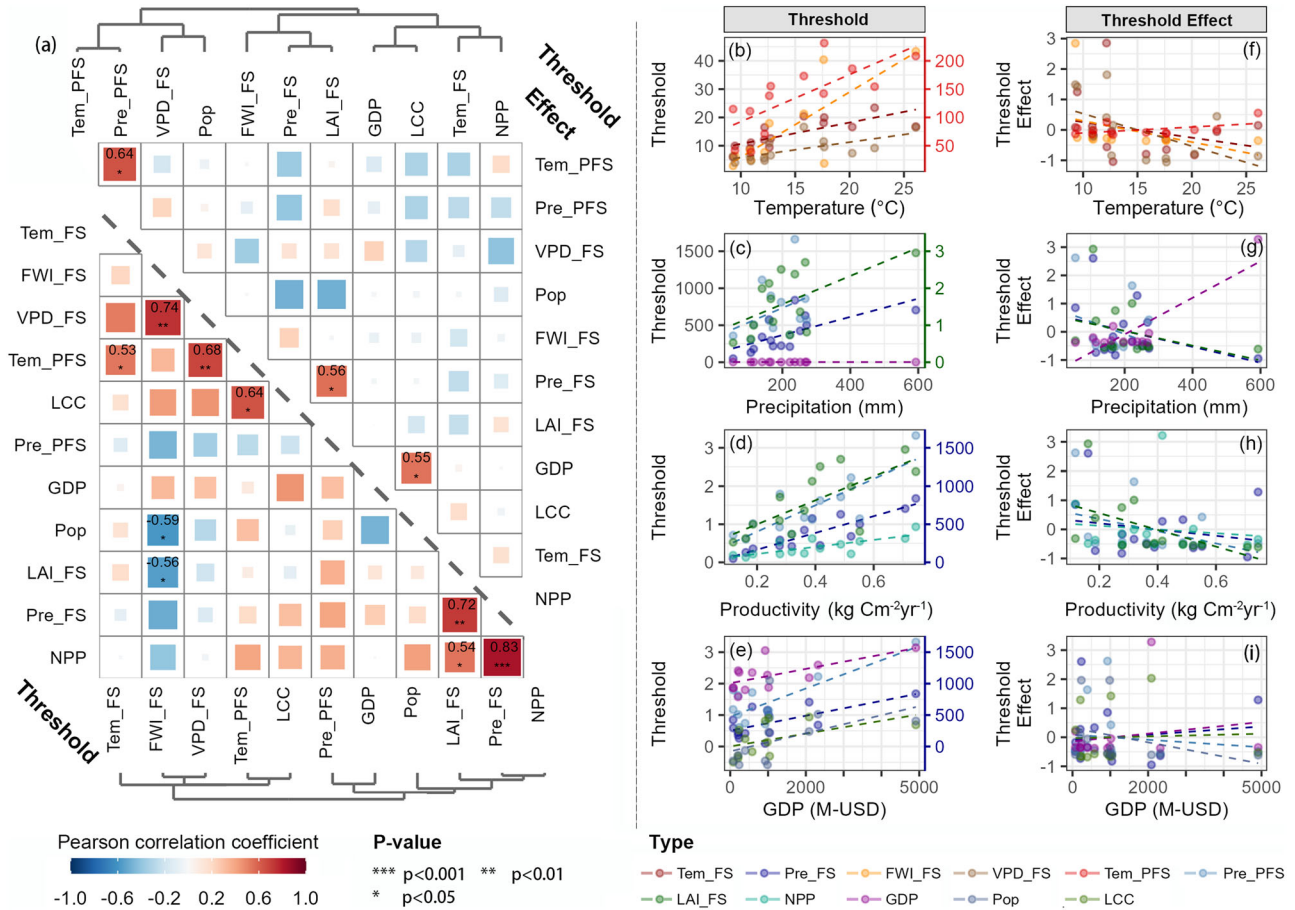
Fig. 2 | Correlations and spatial covariation patterns among thresholds (or threshold effects) of different wildfire drivers. a Lower and upper triangular matrices show the correlation coefficients between the thresholds of wildfire drivers and the correlation coefficients between the threshold effects (absolute value). The binary trees represent cluster relationships among variables. **b–e** depict the linear spatial covariation patterns of the thresholds along spatial gradients (slopes with $p<0.05$), whereas **f–i** illustrate the spatial covariation patterns of the absolute values of threshold effects (z-score scaled). The colors on the right secondary axis correspond to the variable colors. Refer to Supplementary Table 1 for the slopes, R^2, and p values of the linear regression models.

increases were greater in temperate and boreal ecosystems, exceeding 20000–50000 km² in each ecoregion with a percentage increase of less than 50% (Fig. 5g–l). Conversely, BA increments are generally less than 20000 km² in some subtropical and polar ecosystems, with percentage increases ranging from 100% to 250%. Therefore, substantial BA increases will be concentrated in temperate and boreal ecosystems. BA in subtropical and polar ecosystems will exhibit long-term and rapid growth trends, despite relatively smaller BA increases due to smaller land areas.

The contribution of threshold effects to BA will also change by an average of 2.66 to 4.14 percentage points (Supplementary Fig. 12), which will enhance in 21.76% of the land areas and weaken in 17.75% of the land areas under four socio-climatic scenarios (Fig. 6a–f). Notably, the contribution of threshold effects enhanced by more than 15 percentage points in most boreal tundra, temperate steppes, and subtropical moist forests, while it weakened by nearly 10 percentage points in some boreal coniferous forests, subtropical dry forests, and subtropical mountain systems. Although changes in the contribution of threshold effects exhibited similar spatial patterns across different scenarios (Supplementary Fig. 12), they will enhance additionally by 2 ~ 3 percentage points under higher emission scenarios over broader areas. Further analysis showed that changes in future BA have strong positive linear relationships with changes in the contribution of threshold effects (Fig. 6g). The enhanced contribution of threshold effects under climate change was projected to result in a more pronounced increase in BA in boreal mountain systems, temperate grasslands, and temperate and subtropical deserts, nearly doubling the impact compared with that in other ecoregions.

Discussion

The nonlinear threshold relationships between wildfires and their drivers are pervasive and vary regionally, effectively explaining the spatial heterogeneity of wildfire response patterns across ecoregions and similarities within climate zones. Thresholds for most climate drivers are lower and more easily exceeded in polar and boreal ecosystems (Fig. 1a–f), suggesting that even small climate shifts may cause climate drivers to exceed thresholds first and alter wildfire responses[11,15]. This finding provides robust evidence to explain the high sensitivity of high-latitude wildfires to climate change and supports the notion that climatic thresholds shape northern high-latitude fire regimes[4,13]. We also find that increasing precipitation, coupled with drought, vegetation productivity, and human activities that exceed their thresholds, ultimately drive increases in temperate wildfires (Fig. 1b–i). In regions where dry conditions and human ignitions are met, an adequate preseason moisture supply may reduce fuel limitation by improving vegetation productivity[27], thus promoting wildfire changes, especially in arid temperate steppes and desert shrublands[28]. Conversely, subtropical wildfires are seldom limited by fuel and are driven by heat, drought, and socioeconomic factors (Fig. 1d–e, i–k). Therefore, subtropical wildfires rapidly increase once these thresholds are exceeded[29]. However, human control measures have exceeded their thresholds and moderated the changes in subtropical wildfires, especially around densely populated areas, suggesting that sustained and effective interventions help curb the trend of increasing wildfires[30].

The spatial differences and covariation patterns of thresholds are shaped by gradient differences in heat and moisture conditions, vegetation productivity, and human activities (Fig. 2). Wildfire drivers with similar properties
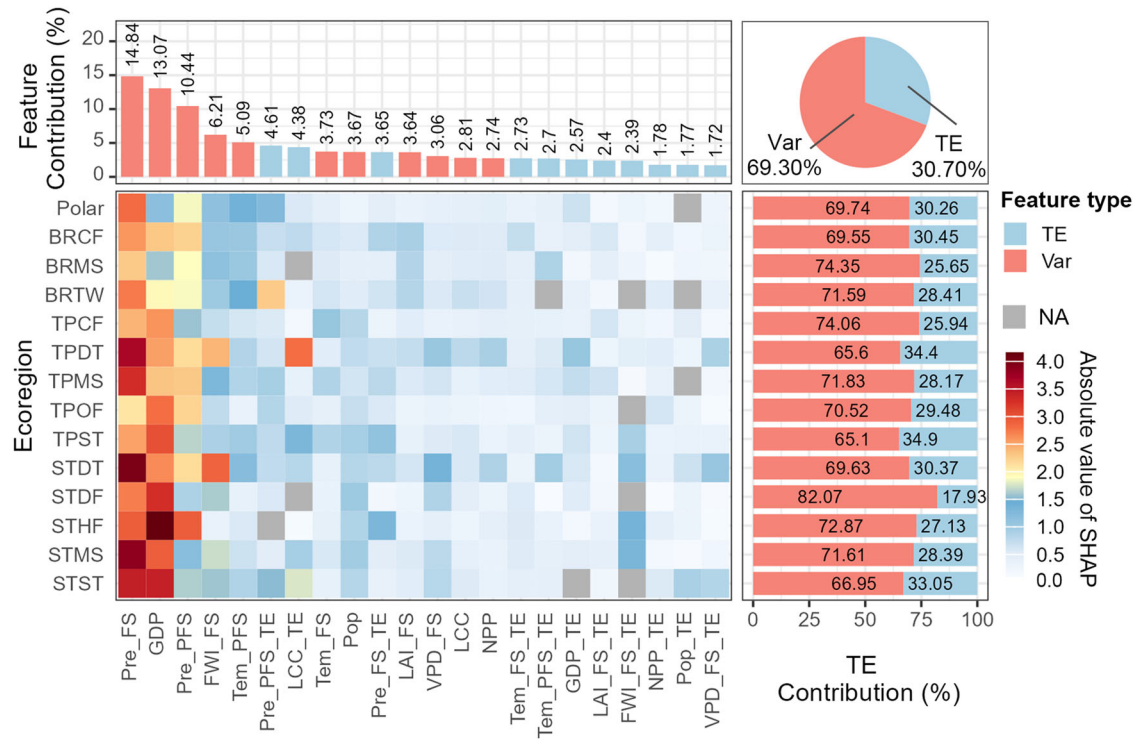
Fig. 3 | The contribution of wildfire drivers and their threshold effects. The heatmap is the absolute Shapley additive explanation value (SHAP) of wildfire drivers and threshold effects in each ecoregion. The bar and pie charts above summarize the total con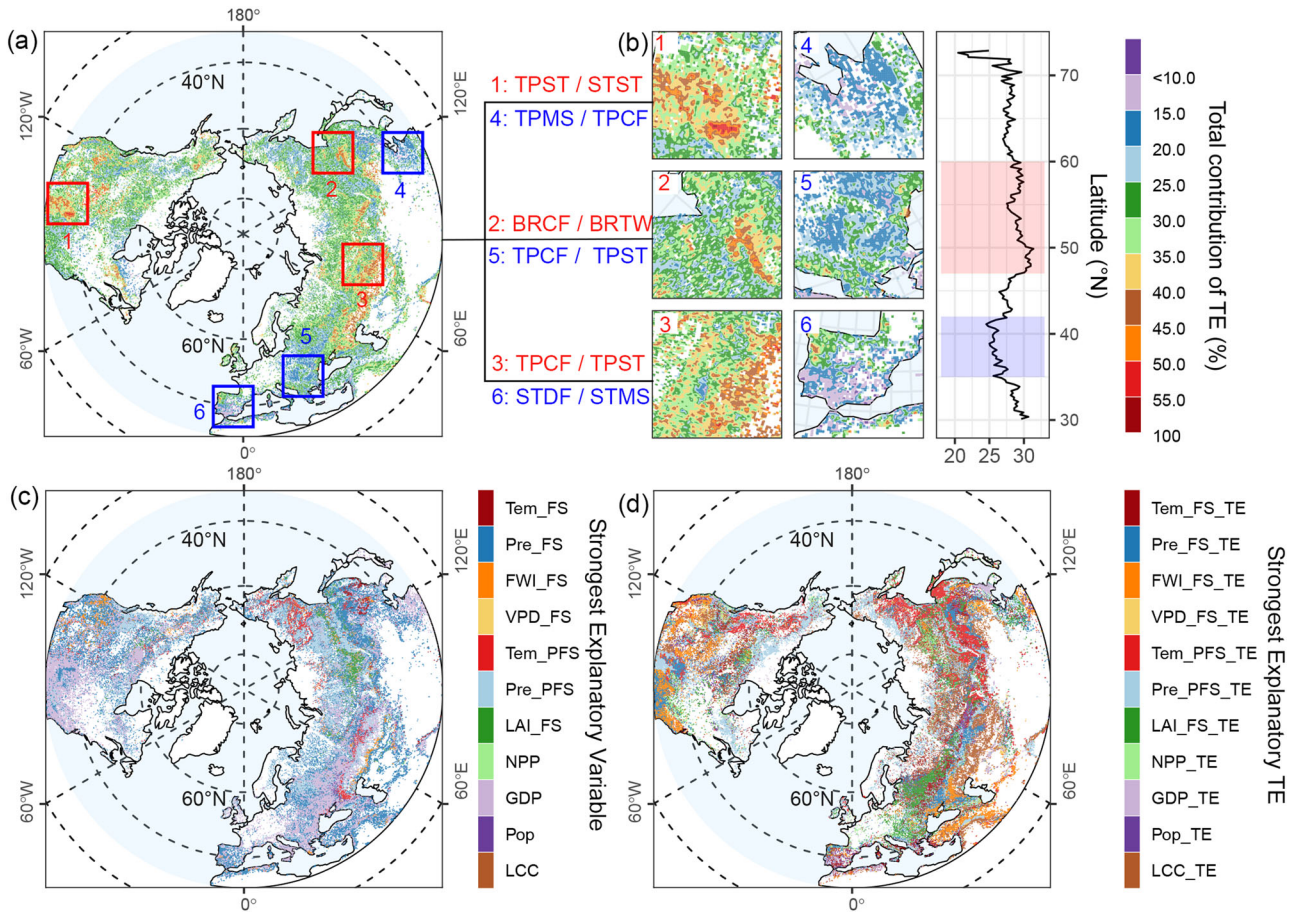tributions of the drivers (Var) and threshold effects (TE). The cumulative bar charts on the right quantify the contribution ratios of drivers and threshold effects in each ecoregion. The variables suffixed with _TE indicate the threshold effects of the corresponding driver.

may reach their thresholds under analogous environmental conditions, leading to comparable spatial patterns. Moreover, regional differences in climate, vegetation, and human activities essentially determine ecosystem stability to control the conditions under which drivers reach thresholds, thereby shaping their spatial covariation patterns. For example, ecosystems with limited heat, moisture, and vegetation tend to have weaker ecosystem stability[1,31], making wildfires more susceptible to external changes and prone to exceeding thresholds related to fuel availability (Fig. 2b–d). Conversely, ecosystems with relatively high thresholds for preseason climates, vegetation productivity, and population generally exhibit relatively strong ecosystem stability[22,27], making wildfires prone to thresholds related to flammability (Fig. 2b, e). More importantly, correlations and covariation patterns among thresholds also suggest that changes in individual drivers may trigger ripple effects of wildfire responses, causing successive exceedances of interconnected thresholds[32]. For example, higher temperatures increased both vapor pressure deficit and pre-season temperature, sequentially triggering their thresholds, as these thresholds are positively correlated and jointly driven by heat variability (Fig. 2a–b). Moreover, their threshold effects may interact with each other to obscure the spatial pattern of threshold effects of individual drivers[32,33]. For example, the negative threshold effects of vapor pressure deficit and preseason temperature partially counterbalance the positive threshold effects of temperature in boreal and polar ecosystems (Fig. 1a, d, e). Consequently, their threshold effects fail to exhibit notable spatial patterns along the heat gradient (Supplementary Table 1). This argument explains our unexpected results—the lack of distinct spatial patterns of the threshold effects along environmental gradients for individual drivers (Fig. 2f–i).

We identified temperature, precipitation, and socioeconomic status as the dominant drivers of mid- and high latitude wildfires (Figs. 3 and 4c). Numerous studies have confirmed that droughts promote wildfires due to rising temperatures and decreasing precipitation[11,26,34]. Conversely, human activities, such as agricultural expansion and intensification or fire suppression, led to decreases in BA[30,35]. Our results also highlight that threshold effects explained roughly one-third of wildfire variability, especially with the

most pronounced impact at northern high latitudes (> 50°N) (Figs. 3 and 4b). Warming and drought have intensified wildfires at high latitudes due to Arctic oscillations, sea-ice loss, and moisture transport changes[20,24,36]. In this context, we argue that temperature, drought, and their threshold effects may interact to facilitate wildfires in high-latitude ecoregions (Fig. 4c–d). For example, threshold effects amplified the promoting effects of warmer and drier conditions on wildfires, leading to an increase in large wildfires[11,37,38]. Conversely, threshold effects had a relatively weaker impact near 40°N (Fig. 4b–d). In these regions, wildfires are influenced primarily by precipitation and GDP, whereas the threshold effects of FWI_FS, LAI_FS, and LCC are weaker and rarely enhance the influence of dominant drivers. These findings extend the current understanding of multifactor threshold effects and interactions between drivers and their threshold effects.

Ongoing climate change is projected to increase the annual mean BA in mid- and high latitudes by 47.81 ± 3.08% from 2030–2100 under socio-climatic scenarios (Fig. 5). This finding was supported by several regional-scale studies, which projected a 3% to 52% increase in California wildfires under warming climates and a 40% to 100% increase in wildfires in Mediterranean Europe under different climate scenarios[39,40]. Importantly, our results highlight that lower emission scenarios can substantially mitigate the long-term increasing trend in wildfires, keeping the overall increase in burned areas to 41% by the end of this century (Fig. 5g–i). Comparatively, the overall increase in burned areas will exceed 55% under higher emission scenarios, posing a substantial threat to boreal ecosystems in particular. In this context, although the burned areas in temperate steppes are expected to continually decrease due to enhanced human control measures (Fig. 5a–f), the mitigating effect on the overall increase in wildfires will be rather limited. Likewise, previous projections for Colorado wildfires indicated BA increases of 39% and 95% by 2100 under RCP4.5 and RCP8.5, respectively, while increases of 22% by 2050 and 11% by 2100 are projected under RCP2.6[41]. Therefore, if human development follows the lower emissions scenarios, the slowdown in the wildfire growth rate will help slow the process of carbon emissions and global warming.

Fig. 4 | Spatial maps of the total contribution of threshold effects and the most important drivers and threshold effects. a Total contribution of the threshold effects. **b** Enlarged views of six regions with the highest and lowest contributions. The latitudinal profile of the contribution of threshold effects and the highest and lowest ranges are shown. **c, d** Spatial patterns of drivers and threshold effects that contribute the most to wildfires.

Climate change will promote future wildfire changes in mid- and high latitudes by enhancing the contribution of threshold effects to wildfires (Fig. 6). Wildfires in temperate and boreal ecosystems contribute to more than 80% of burned areas in northern mid- and high latitudes (Supplementary Fig. 13c–d) and are more sensitive to climate change and susceptible to threshold effects. Therefore, minor climate change is sufficient to cause widespread and substantial increases in wildfires, even with a relatively slight enhancement of the threshold effects due to climate change[11,15]. This explanation fits with our results that wildfires in these ecosystems will considerably increase but have a lower overall increment rate under climate change (Fig. 5g–l). Subtropical ecosystems, accounting for approximately 18% of wildfires, showed strong and positive linear relationships between enhanced threshold effects and increasing BA (Fig. 6). Wildfires in subtropical ecosystems also exhibited a minor increment but a more substantial overall change rate (Fig. 5g–l). A possible explanation is that climate change strengthened the role of threshold effects in wildfire responses (Fig. 6g), thereby increasing the variability of subtropical wildfires[21,42,43]. These findings suggest that the nonlinear response of wildfires to external changes due to threshold relationships will pose great challenges for future wildfire prediction and land management.

Our insights into threshold effects and future wildfire changes have three limitations. First, threshold effects are inherent properties of wildfire response and theoretically depend entirely on ecosystem characteristics and the intensity of external disturbances. However, data quality, spatial scales, and parametric models may introduce noise and lead to the identification of 'pseudo-thresholds' that lack ecological significance[44,45]. While bootstrap and comparison tests provide statistical reliability measures for our estimates, validation through empirical experience remains indispensable.

Second, we used thresholds obtained from the early 21st century and assumed their robustness in the future. However, ecosystem adaptation to climate change, vegetation feedback, and shifts in human development concepts may alter these threshold parameters, introducing nonstationarity into the established relationships[4,46,47]. Meanwhile, such changes may also potentially trigger additional drivers of otherwise linear changes to exhibit nonlinearity and threshold effects in the future, complicating the identified multifactor interactions. Finally, although we have validated the performance of GCMs in climate change projections by considering their uncertainty (Supplementary Note 2), the inherent differences between GCMs may affect our projections[48], which are determined by their initial parameters.

In conclusion, this study offers key insights into the role of threshold effects in controlling both present and future changes in wildfire dynamics. We identify key thresholds where relationships between wildfires and their drivers shift, revealing the widespread nonlinear response of wildfires to environmental changes. Our findings suggest that the geographical difference in thresholds effectively explains spatial patterns of the wildfires and their uneven responses, and the threshold effects of drivers overall contribute to roughly one-third of wildfire variability in northern mid- and high latitudes. More notably, climate change will enhance the impact of threshold effects on wildfires to exacerbate variability in future wildfires. By the end of this century, burned areas in mid- and high latitudes will increase by at least 41% under low emissions scenarios and by more than 55% under high emissions scenarios. Wildfire dynamics in mid- and high latitudes will be more variable under climate change due to the nonlinear threshold relationships between wildfires and drivers, challenging future wildfire management and risk assessment. This study gives added importance to
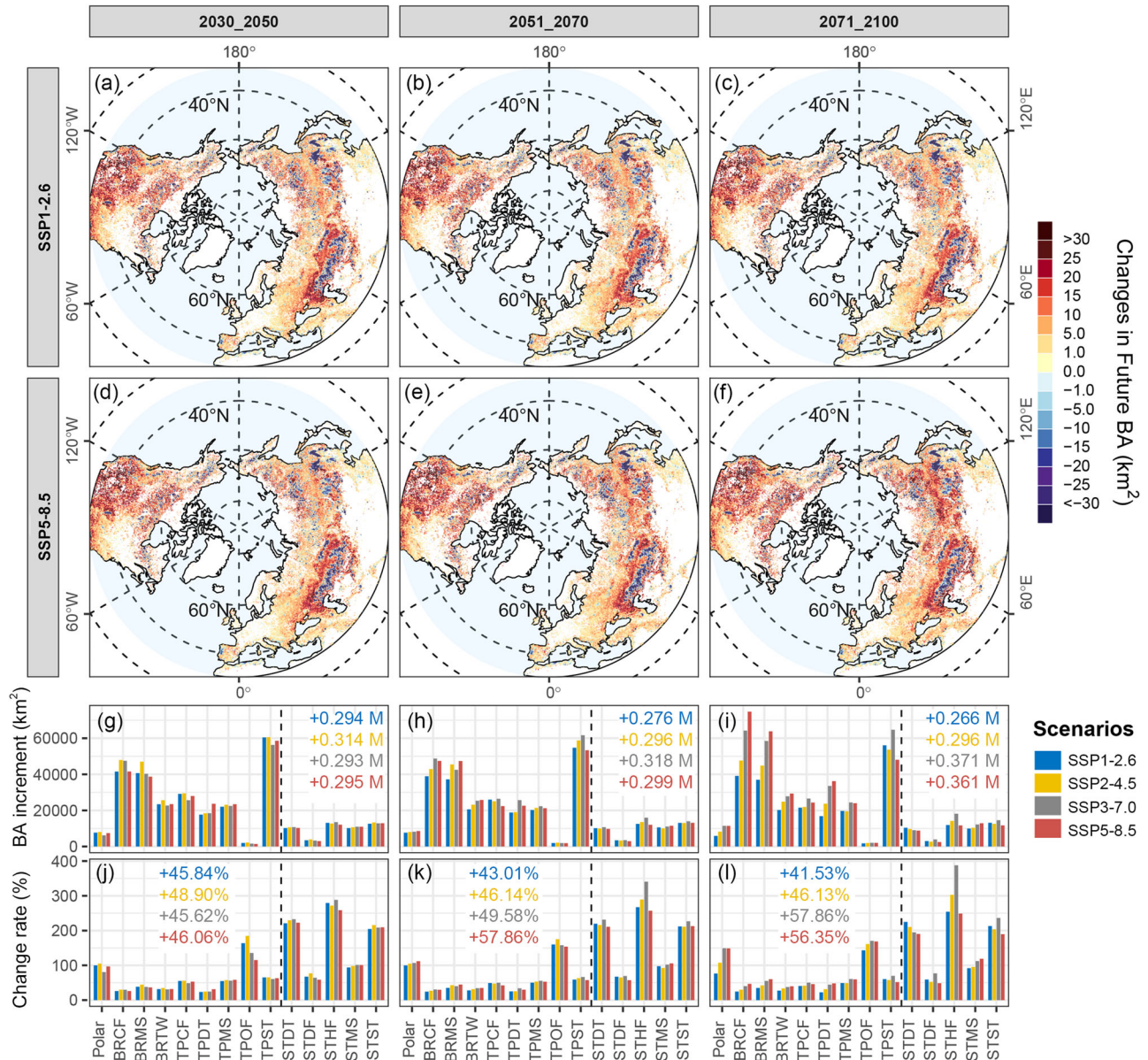
Fig. 5 | Future changes in BA during the fire seasons under four socio-climatic scenarios. Compared with the annual mean BA of the historical period (2001–2022), **a–f** show the spatial distributions of changes in BA under the SSP1-2.6 and SSP5-8.5 scenarios in 2030–2050, 2051–2070, and 2071–2100. Similar spatial distribution patterns were observed under the SSP2-4.5 and SSP3-7.0 scenarios, as shown in Supplementary Fig. 11. Panels **g–i** and **j–l** illustrate the increment (labeled with million km²) and rate of change (%) in the future BA at the ecoregion scale.

understanding nonlinear wildfire response mechanisms and provides a theoretical basis for formulating tailored policies for fire suppression, land management, and climate change adaptation.

Methods

Remote sensing-based burned area dataset

We used the European Space Agency (ESA) FireCCI51 dataset and the Moderate Resolution Imaging Spectroradiometer (MODIS) MCD64A1 dataset to construct a monthly time series of burned areas from 2001 to 2022 (Supplementary Table 3). The FireCCI51 dataset integrates the standard MODIS BA product into a 0.25° monthly gridded dataset and offers pre-fire land cover categories for the burned pixels[49,50]. Since the FireCCI51 dataset was only updated to 2020, we extended the BA time series to 2022 via methodologies similar to those used by the dataset producers. We performed this extension on the Google Earth Engine platform using the 500 m MCD64A1 dataset from 2021–2022[51] and the latest-updated land cover

category of 2020 from the Land Cover CCI project[52]. Notably, although BA has high spatiotemporal consistency between the MCD64A1 and FireCCI51 datasets[53], our extended method may underestimate BA in both years. This is because FireCCI51 uses an updated BA detection algorithm that is more sensitive to small fires, thus reducing BA underestimation[50]. However, since multiyear average BA was ultimately used for analysis, the potential impact of this discrepancy on our results is relatively limited. The original BA dataset excluded unburnable areas, such as water, bare land, urban, and permanent ice and snow-covered areas, and we further excluded BA in croplands. This exclusion was driven by the substantial underestimation of cropland BA, attributed to high commission and omission errors (49% and 63%) in moderate-resolution satellite detection for crop fires[54].

Historical observation datasets

Climate datasets were obtained from the ERA5 reanalysis dataset of the European Center for Medium-Range Weather Forecasts (ECMWF), which
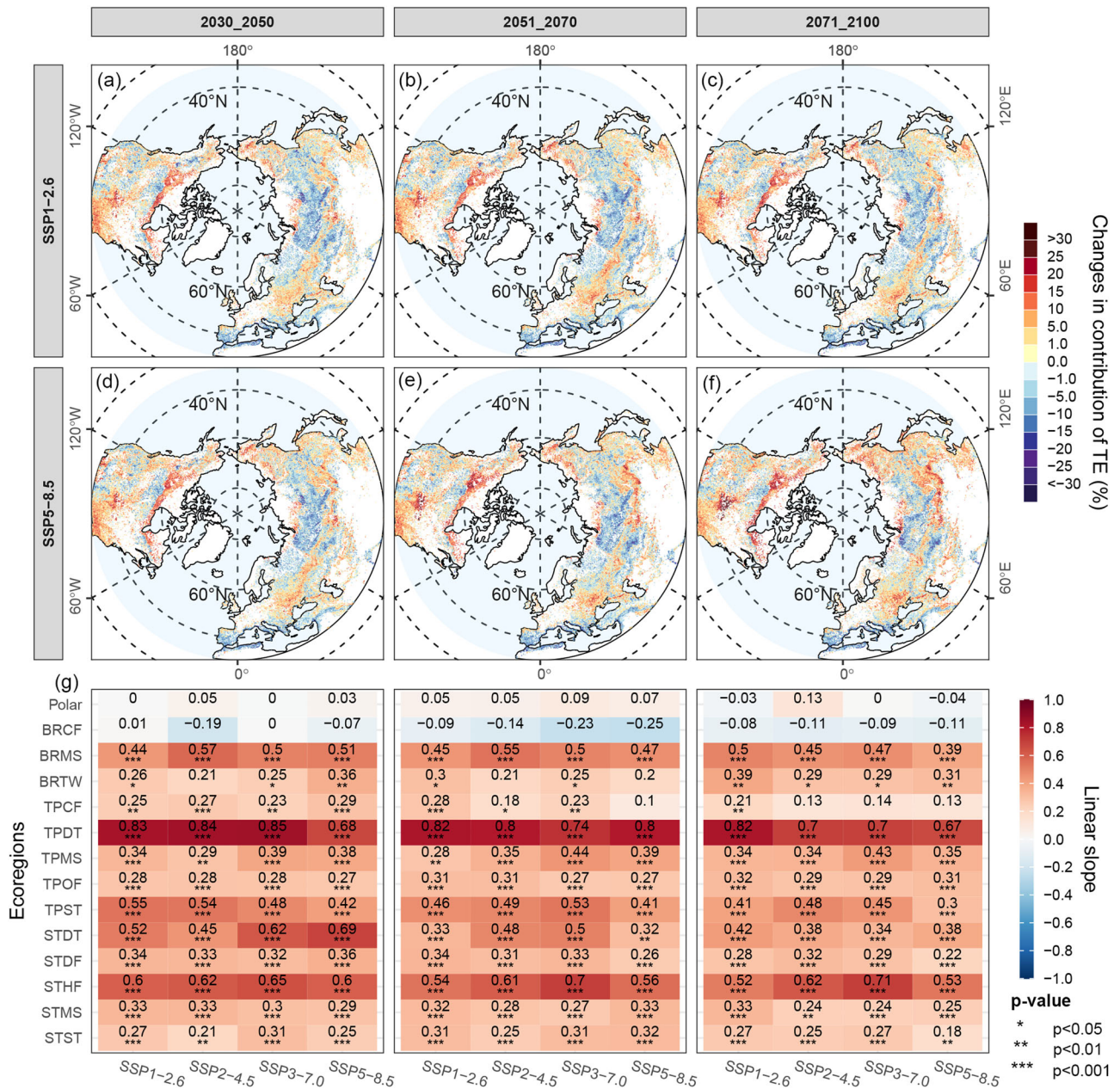
Fig. 6 | Future changes in the contribution of threshold effects under socio-climatic scenarios during three periods. a–f Spatial distribution of the changes in the contribution of threshold effects (%, percentage points). Similar spatial distribution patterns were observed under the SSP2-4.5 and SSP3-7.0 scenarios, as shown in Supplementary Fig. 12. **g** Bootstrap slopes of the simple linear regression between changes in BA and changes in the contribution of threshold effects in each ecoregion.

range from 2000 to 2022 and have a 0.25° spatial resolution[55]. We selected 2 m air temperature and total precipitation to measure heat and moisture conditions and combined them with 2 m dewpoint temperature to calculate the atmospheric vapor pressure deficit (VPD) from the ERA5 dataset[56]. A public averaged monthly fire weather index (FWI) dataset from 2002 to 2020, developed from the ERA5 reanalysis dataset, was also employed to obtain a climatic indicator characterizing potential fire risk[57]. We extended this dataset to 2022 by calculating monthly FWI using the methods provided by dataset producers, the ERA5 hourly dataset, and the Canadian Fire Weather Index System.

We also used other MODIS products, including annual net primary production, the 8-day leaf area index (LAI), and annual plant functional type (PFT)[58–60]. The first two datasets, ranging from 2001 to 2022, were resampled to 0.25° spatial resolution to estimate vegetation productivity, and the LAI dataset was further averaged by timestamp to create a monthly

time series. We defined the rate of land cover change (LCC) as the proportion of pixels showing changes in PFT within a 0.25° grid cell between adjacent years. A 0.25° LCC dataset from 2002 to 2021 was subsequently constructed to quantify the magnitude of land cover change, in which the LCC of 2022 was substituted with the LCC of 2021, as the latest PFT dataset was only updated to 2021. Population and gross domestic product datasets were used to characterize socioeconomic development and the intensity of human activity. A population dataset with a 1-km spatial resolution ranging from 2000 to 2022 was obtained from the LandScan program[61]. We also used a global 1-km gridded revised real gross domestic product from 2001 to 2019 and extended this dataset to 2022[62]. Specifically, we developed a simple linear regression model using available time series data at the pixel scale and interpolated GDP values from 2020 to 2022 based on the model parameters obtained. Both datasets were aggregated over a 0.25 grid to match the resolutions of the other spatial datasets.
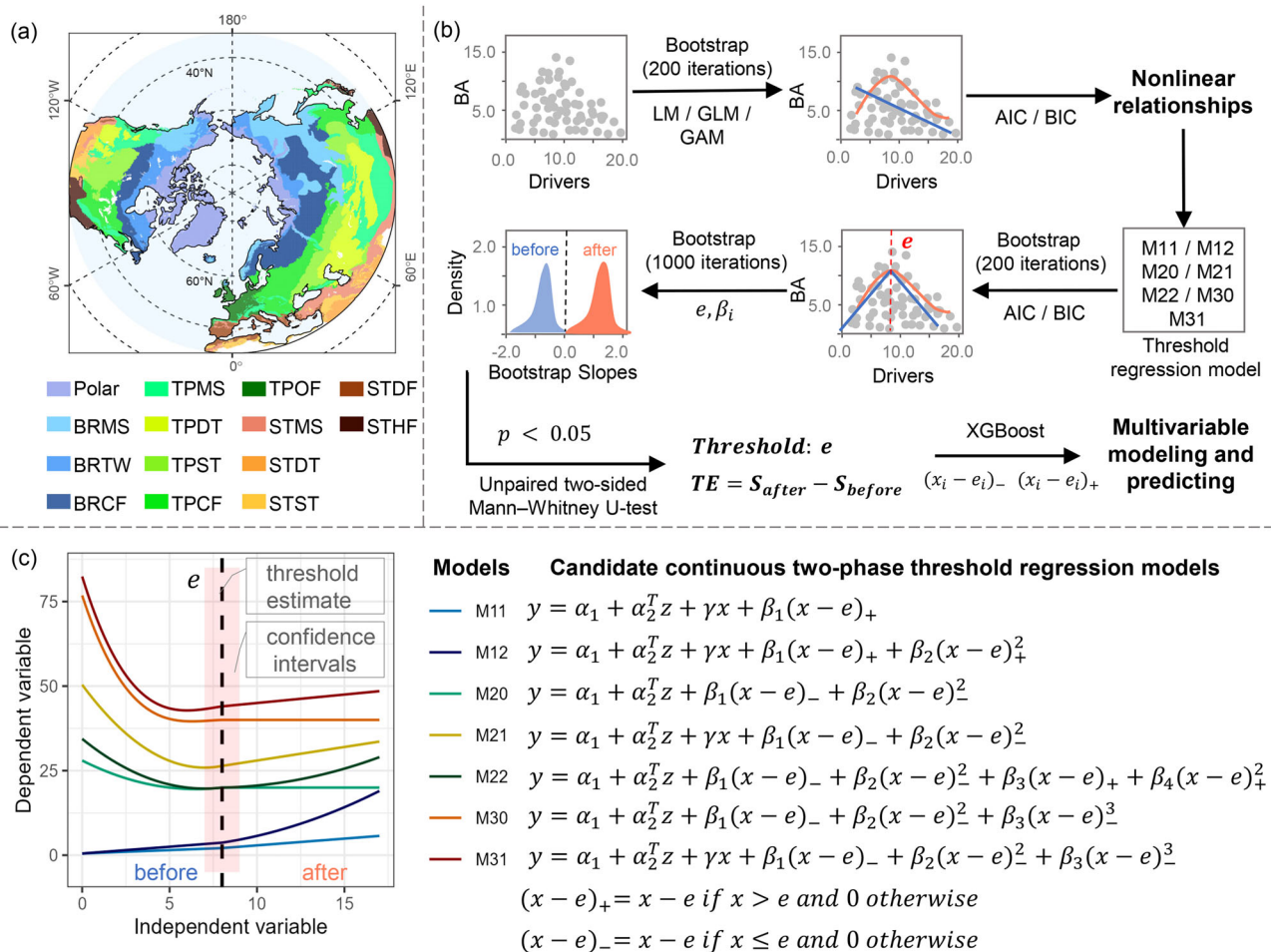
Fig. 7 | Workflow for identifying threshold effects with an introduction to threshold regression models. a Ecoregions of northern mid- and high latitudes. **b** Workflow for identifying nonlinear relationships, thresholds, and threshold effects. **c** Candidate threshold regression models, where e is the threshold parameter, x is the predictor with threshold effects, and z is a vector of additional predictors. Any parameters in this panel are hypothetical representations of the threshold regression model and are not related to the initial values.

An ecoregion map with climate zones from the Food and Agriculture Organization of the United Nations was also incorporated (Supplementary Table 3). Our study area included 14 ecoregions north of 30°N, excluding tropical ecoregions (Fig. 7a): polar (Polar), boreal mountain system (BRMS), boreal tundra woodland (BRTW), boreal coniferous forest (BRCF), temperate mountain system (TPMS), temperate desert (TPDT), temperate steppe (TPST), temperate continental forest (TPCF), temperate oceanic forest (TPOF), subtropical mountain system (STMS), subtropical desert (STDT), subtropical steppe (STST), subtropical dry forest (STDF), and subtropical humid forest (STHF).

Future simulation datasets under socio-climatic scenarios
The future simulation dataset includes nine sub-datasets, each offering the same types of base variables as the historical dataset (Supplementary Table 3). We chose six general circulation models (GCMs) from the Coupled Model Intercomparison Project Phase 6 (CMIP6)[63]. These models provide monthly future simulation datasets of temperature, dewpoint temperature, total precipitation, seasonal average FWI, the leaf area index, and net primary production from 1960 to 2100 under four shared socio-economic pathways (SSP1-2.6, SSP2-4.5, SSP3-7.0, and SSP5-8.5) (Supplementary Fig. 14; Supplementary Table 4). Supplementary Note 2 provides detailed information on the selection and validation of these GCMs. In addition, we incorporated three public datasets that offer simulation datasets of population, gross domestic product, and plant functional types from 2015 to 2100 under shared socioeconomic pathways[64–66]. Since

the spatial resolutions of these future simulation datasets vary (100–250 km), we aggregated them to a uniform 0.25° spatial resolution. The same pretreatment methods as those used for the historical datasets were applied to create future simulation datasets.

Extracting wildfire drivers and creating modeling datasets
The seasonality and duration of wildfires vary across regions due to the spatial heterogeneity of climatic and human factors. We defined the fire season (FS) as the briefest adjacent calendar months (intervals of less than three months) within a fire year that encompasses more than 80% of the BA[67]. We also defined the preseason (PFS) as the 3 to 14 months before the onset of the fire season, considering that antecedent climate can influence subsequent wildfires with lag effects of up to two years[14,68]. A two-month buffer before the onset of the fire season was set to avoid confusion between the preseason and fire season climates that directly affect flammability. We ultimately calculated the multiyear average BA for each of the 12 calendar months from 2001 to 2022 to identify the fire year and fire-prone months at the pixel scale, thereby extracting a broad and stable fire season for each grid cell (Supplementary Fig. 13a–b). We assumed that the fire season would remain constant in the future. This assumption reduces the influence of fire season variability on BA projections and comparisons, thereby facilitating the identification of threshold effects in wildfire changes.

We used the BA during fire season (BA_FS) as the target variable. Mean temperature (Tem_FS), total precipitation (Pre_FS), average monthly FWI (FWI_FS), and vapor pressure deficit (VPD_FS) were each aggregated

as seasonal explanatory variables to characterize the climatic conditions during the fire season. Preseason climate impacts on wildfires were gauged using preseason temperature (Tem_PFS) and preseason precipitation (Pre_PFS), which were defined as the sum of monthly average temperature exceeding 5 °C and total precipitation during the preseason, respectively. Here, 5 °C is the minimum temperature required for most plants to accumulate nutrients. The average leaf area index in the fire season (LAI_FS) and annual total net primary production (NPP) served as proxies for vegetation productivity controlling fuel loading and allocation. Anthropogenic controls included population (Pop), gross domestic product (GDP), and the land cover change rate (LCC) to quantify socioeconomic and human factors, and they were log-transformed to mitigate skewness and reduce the data range. The annual time series of these indicators were then extracted to calculate multiyear averages. We converted historical multiyear averages (2001–2022) to a modeling dataset and randomly divided it into training, validation, and testing sets at a ratio of 6:2:2. Additionally, we created twelve future simulation datasets for three periods (2030–2050, 2051–2070, and 2071–2100) under four future scenarios simultaneously.

Identifying and analyzing the threshold effects of wildfire drivers

The nonlinear threshold relationships between wildfires and drivers were explored using threshold regression models, which incorporate a threshold parameter (e) and segmented regression models to interpret nonlinearity[44,69]. We merged the training and validation set to fit the models and assessed model performance using the testing set. The samples extracted from the gridded data exhibited spatial autocorrelation, violating the independence assumption for statistical modeling. Thus, we applied bootstrap and stratified sampling to mitigate spatial autocorrelation. Moreover, model comparison and selection relied on the Akaike information criterion (AIC) and Bayesian information criterion (BIC).

We first modeled the bivariate relationship between BA_FS and each wildfire driver within each ecoregion using a linear model (LM), generalized linear model (GLM), and generalized additive model (GAM) to identify linear or nonlinear relationships (Fig. 7a, b). A threshold may exist in the nonlinear relationships only if nonlinear regressions (GLM and GAM) were the "optimal model" with the lowest AIC and BIC values. Second, we selected the best-fitting threshold regression model with the lowest AIC or BIC values from seven candidate continuous two-phase threshold regression models to parameterize the nonlinear threshold relationships (Fig. 7c). Third, this final threshold regression model was fit to obtain the estimates of the threshold with 95% confidence intervals and the slopes before and after thresholds by performing 1000 bootstrap samplings. Here, threshold (e) is defined as the position on the x-axis, where the nonlinear relationship between wildfire (y-axis) and the driver (x-axis) abruptly shifts. The threshold effect (TE) is defined as the overall change in slope after the driver crosses this threshold. A positive value indicates that wildfire changes are enhanced after the driver exceeds the threshold (enhancing effect), while a negative value suggests a weakened wildfire change (weakening effect). Finally, bootstrap slopes before and after the threshold were compared with an unpaired two-sided Mann‒Whitney U test ($p<0.05$) to ensure the validity of the identified threshold and quantify the strength and direction of threshold effects.

We analyzed the spatial patterns of thresholds across ecoregions by examining correlations between different thresholds of wildfire drivers and linking these patterns to environmental gradients. Specifically, Pearson's correlation coefficients were calculated to examine the relationships between thresholds (or threshold effects) of different drivers at the ecoregion scale. Significant correlations indicated that these thresholds (or their threshold effects) exhibited analogous spatial patterns across ecoregions. We calculated the averages of Tem_FS, Pre_FS, NPP, and GDP to create gradients of heat, moisture, vegetation productivity, and socioeconomic development, which serve as proxies for differences in geographic contexts across ecoregions. We then analyzed the spatial covariation patterns of different thresholds along gradients when significant correlations were identified. The latitudinal profiles of the thresholds were also illustrated to reveal their latitudinal change patterns. Similarly, the spatial patterns of threshold effects were analyzed using the same methods.

Quantifying the contributions of drivers and threshold effects on wildfires

The extreme gradient boosting (XGBoost) model was employed to quantify the impacts of multifactors and their threshold effects on wildfires[70]. Inspired by threshold regression modeling, we created two new features, $(x - e)_+$ and $(x - e)_-$, for the corresponding driver, when a significant threshold relationship was identified in an ecoregion. They measure threshold effects following the formula from the selected threshold regression models (Fig. 7c). Consequently, a total of 33 features (independent variables) and BA_FS (dependent variable) were used for multivariable modeling. We trained an initial XGBoost model on the training set and fine-tuned its hyperparameters via Bayesian optimization on the validation set. The effectiveness and robustness of the optimized XGBoost model were assessed using root mean squared error (RMSE) on a testing set. The Shapley additive explanation value (SHAP) was employed to estimate the contributions of wildfire drivers and threshold effects in the XGBoost model. SHAP values interpret machine learning outcomes by measuring each feature's or sample's contribution to the predictions[71]. The contribution of threshold effects was determined by the absolute SHAP value of the difference between $(x - e)_+$ and $(x - e)_-$. The strongest explanatory variable and key threshold effects across ecoregions were also identified to analyze their spatial heterogeneity. The source data, codes, and core outputs to implement the model were publicly accessible in Figshare[72].

Projecting changes in wildfires and threshold effects under climate change

The future BA of the fire season during three periods (2030–2050, 2051–2070, and 2071–2100) were projected using the validated XGBoost model under four socio-climatic scenarios (SSP1-2.6, SSP2-4.5, SSP3-7.0, and SSP5-8.5). Due to the limitations of fire seasons obtained from remote-sensing data, we only projected the future BA on the land areas (or pixels) where wildfires occurred in the past. We then quantified BA changes relative to the historical period (2001–2022) at both the ecoregion scale and the pixel scale to reveal the change characteristics of future wildfires in the context of climate change. Changes in the contributions of wildfire drivers and their threshold effects were also estimated using the SHAP value. To understand how changes in the contribution of threshold effects contribute to future wildfire changes, we further calculated the slope of a simple linear regression model between BA changes and contribution changes in threshold effects at the pixel scale for each ecoregion. Here, bootstrap sampling was used to reduce the influence of spatial autocorrelation on correlations by randomly selecting 500 sparse samples from each ecoregion, thereby estimating their slopes and significance after 100 iterations.

Data availability

FireCCI51 and ESA CCI-LC datasets were obtained from the European Space Agency's Climate Change Initiative (https://climate.esa.int/en/projects/). MODIS products, including MCD64A (burned areas), MYD17A3HGF (Net Primary Production), MOD15A2H (Leaf Area Index), and MCD12Q1 (Plant Functional Types), were obtained from the National Aeronautics and Space Administration (NASA) (https://search.earthdata.nasa.gov/search). Historical climate data were derived from the ERA5 reanalysis datasets of the European Center for Medium-Range Weather Forecasts (ECMWF) (https://cds.climate.copernicus.eu/datasets). Global ecological zones were provided by the Food and Agriculture Organization (https://www.fao.org/forest-resources-assessment/remote-sensing/). Population data were obtained from the LandScan Program of Oak Ridge National Laboratory (https://landscan.ornl.gov/). Global gross domestic product dataset (https://doi.org/10.6084/m9.figshare.17004523.v1) and future global population distributions dataset (https://doi.org/10.6084/m9.figshare.19609356.v3) are available from Figshare. CMIP6 model outputs are available via the Earth System Grid Foundation (ESGF) (https://

aims2.llnl.gov/search/cmip6/). Global fire weather indices (https://doi.org/10.5281/zenodo.3626193), future gross domestic product (https://doi.org/10.5281/zenodo.7898409), and future global plant functional type (https://doi.org/10.5281/zenodo.4584775) are publicly available from Zenodo. All datasets and their details are listed in the Supplementary information (Supplementary Table 3).

Code availability

All analysis was conducted in R version 4.2. Open-source R packages are listed in the supplementary information (Supplementary Table 5). The source data and codes that support the findings of this study are available in Figshare (https://doi.org/10.6084/m9.figshare.28171160).

References

1. Suding, K. N. & Hobbs, R. J. Threshold models in restoration and conservation: a developing framework. *Trends Ecol. Evolution* **24**, 271–279 (2009).
2. Hillebrand, H. et al. Thresholds for ecological responses to global change do not emerge from empirical data. *Nat. Ecol. Evolution* **4**, 1502–1509 (2020).
3. Groffman, P. M. et al. Ecological Thresholds: The Key to Successful Environmental Management or an Important Concept with No Practical Application? *Ecosystems* **9**, 1–13 (2006).
4. Young, A. M. et al. Consequences of climatic thresholds for projecting fire activity and ecological change. *Glob. Ecol. Biogeogr.* **28**, 521–532 (2019).
5. Berdugo, M. et al. Global ecosystem thresholds driven by aridity. *Science* **367**, 787–790 (2020).
6. Feng, Y. et al. Temperature thresholds drive the global distribution of soil fungal decomposers. *Glob. Change Biol.* **28**, 2779–2789 (2022).
7. Archibald, S., Roy, D. P., Van Wilgen, B. W. & Scholes, R. J. What limits fire? An examination of drivers of burnt area in Southern Africa. *Glob. Change Biol.* **15**, 613–630 (2009).
8. Pausas, J. G. & Paula, S. Fuel shapes the fire–climate relationship: evidence from Mediterranean ecosystems. *Glob. Ecol. Biogeogr.* **21**, 1074–1082 (2012).
9. Slocum, M. G., Beckage, B., Platt, W. J., Orzell, S. L. & Taylor, W. Effect of Climate on Wildfire Size: A Cross-Scale Analysis. *Ecosystems* **13**, 828–840 (2010).
10. Peters, D. P. et al. Cross-scale interactions, nonlinearities, and forecasting catastrophic events. *Proc. Natl. Acad. Sci.* **101**, 15130–15135 (2004).
11. Descals, A. et al. Unprecedented fire activity above the Arctic Circle linked to rising temperatures. *Science* **378**, 532–537 (2022).
12. Post, E. & Mack, M. C. Arctic wildfires at a warming threshold. *Science* **378**, 470–471 (2022).
13. Young, A. M., Higuera, P. E., Duffy, P. A. & Hu, F. S. Climatic thresholds shape northern high-latitude fire regimes and imply vulnerability to future climate change. *Ecography* **40**, 606–617 (2017).
14. Alvarado, S. T., Andela, N., Silva, T. S. F., Archibald, S. & Poulter, B. Thresholds of fire response to moisture and fuel load differ between tropical savannas and grasslands across continents. *Glob. Ecol. Biogeogr.* **29**, 331–344 (2019).
15. Senande-Rivera, M., Insua-Costa, D. & Miguez-Macho, G. Spatial and temporal expansion of global wildland fire activity in response to climate change. *Nat. Commun.* **13**, 1208 (2022).
16. Ellis, T. M., Bowman, D. M. J. S., Williamson, G. J. Global variation in ecoregion flammability thresholds. *Ecography* **2024**, e07127 (2024).
17. Benyon, R. G., Inbar, A., Sheridan, G. J. & Lane, P. N. J. Critical climate thresholds for fire in wet, temperate forests. *For. Ecol. Manag.* **537**, 120911 (2023).
18. Hu, F. S. et al. Arctic tundra fires: natural variability and responses to climate change. *Front. Ecol. Environ.* **13**, 369–377 (2015).
19. Cunningham, C. X., Williamson, G. J., Bowman, D. Increasing frequency and intensity of the most extreme wildfires on Earth. *Nature Ecol. Evol.* **8**, 1420–1425 (2024).
20. Luo, B. et al. Rapid summer Russian Arctic sea-ice loss enhances the risk of recent Eastern Siberian wildfires. *Nat. Commun.* **15**, 5399 (2024).
21. Chuvieco, E. et al. Human and climate drivers of global biomass burning variability. *Sci. Total Environ.* **779**, 146361 (2021).
22. Bedia, J. et al. Global patterns in the sensitivity of burned area to fire-weather: Implications for climate change. *Agric. For. Meteorol.* **214-215**, 369–379 (2015).
23. Higuera, P. E. et al. Frequent fires in ancient shrub tundra: implications of paleorecords for arctic environmental change. *PLoS One* **3**, e0001744 (2008).
24. Zhu, X., Xu, X. & Jia, G. Asymmetrical Trends of Burned Area Between Eastern and Western Siberia Regulated by Atmospheric Oscillation. *Geophys. Res. Lett.* **48**, e2021GL096095 (2021).
25. Zheng, B. et al. Record-high CO(2) emissions from boreal fires in 2021. *Science* **379**, 912–917 (2023).
26. Jones, M. W. et al. Global and Regional Trends and Drivers of Fire Under Climate Change. *Rev. Geophys* **60**, e2020RG000726 (2022).
27. Resco De Dios, V. et al. Convergence in critical fuel moisture and fire weather thresholds associated with fire activity in the pyroregions of Mediterranean Europe. *Sci. Total Environ.* **806**, 151462 (2021).
28. Zhao, H. et al. The spatial patterns of climate-fire relationships on the Mongolian Plateau. *Agric. For. Meteorol.* **308–309**, 108549 (2021).
29. Wei, P. et al. Vegetation-fire feedbacks increase subtropical wildfire risk in scrubland and reduce it in forests. *J. Environ. Manag.* **351**, 119726 (2024).
30. Andela, N. et al. A human-driven decline in global burned area. *Science* **356**, 1356–1362 (2017).
31. Ahmad, S. K. et al. Droughts impede water balance recovery from fires in the Western United States. *Nat. Ecol. Evolution* **8**, 229–238 (2024).
32. Rocha, J. C., Peterson, G., Bodin, O. & Levin, S. Cascading regime shifts within and across scales. *Science* **362**, 1379–1383 (2018).
33. Kelley, D. I. et al. How contemporary bioclimatic and human controls change global fire regimes. *Nat. Clim. Change* **9**, 690–696 (2019).
34. Luo, K., Wang, X., de Jong, M. & Flannigan, M. Drought triggers and sustains overnight fires in North America. *Nature* **627**, 321–327 (2024).
35. Kolden, C. A., Abatzoglou, J. T., Jones, M. W. & Jain, P. Wildfires in 2023. *Nat. Rev. Earth Environ.* **5**, 238–240 (2024).
36. Zheng, B. et al. Increasing forest fire emissions despite the decline in global burned area. *Sci. Adv.* **7**, eabh2646 (2021).
37. Kim, J. S., Kug, J. S., Jeong, S. J., Park, H. & Schaepman-Strub, G. Extensive fires in southeastern Siberian permafrost linked to preceding Arctic Oscillation. *Sci. Adv.* **6**, eaax3308 (2020).
38. Liang, L., Liang, S. & Zeng, Z. Extreme climate sparks record boreal wildfires and carbon surge in 2023. *Innov. ((Camb.))* **5**, 100631 (2024).
39. Turco, M. et al. Exacerbated fires in Mediterranean Europe due to anthropogenic warming projected with non-stationary climate-fire models. *Nat. Commun.* **9**, 3821 (2018).
40. Turco, M. et al. Anthropogenic climate change impacts exacerbate summer forest fires in California. *Proc. Natl. Acad. Sci.* **120**, e2213815120 (2023).
41. Silva, P. S., Bastos, A., Libonati, R., Rodrigues, J. A. & DaCamara, C. C. Impacts of the 1.5°C global warming target on future burned area in the Brazilian Cerrado. *For. Ecol. Manag.* **446**, 193–203 (2019).
42. Zhao, Z., Lin, Z., Li, F. & Rogers, B. M. Influence of atmospheric teleconnections on interannual variability of Arctic-boreal fires. *Sci. Total Environ.* **838**, 156550 (2022).
43. Zhuang, Y., Fu, R., Santer, B. D., Dickinson, R. E. & Hall, A. Quantifying contributions of natural variability and anthropogenic forcings on

increased fire weather risk over the western United States. *Proc. Natl. Acad. Sci.* **118**, e2111875118 (2021).

44. Fong, Y., Huang, Y., Gilbert, P. B. & Permar, S. R. chngpt: threshold regression model estimation and inference. *BMC Bioinforma.* **18**, 454 (2017).

45. Son, H. & Fong, Y. Fast grid search and bootstrap-based inference for continuous two-phase polynomial regression models. *Environmetrics* **32**, e2664 (2021).

46. Bueno de Mesquita, C. P., White, C. T., Farrer, E. C., Hallett, L. M. & Suding, K. N. Taking climate change into account: Non-stationarity in climate drivers of ecological response. *J. Ecol.* **109**, 1491–1500 (2021).

47. Littell, J. S., McKenzie, D., Wan, H. Y. & Cushman, S. A. Climate Change and Future Wildfire in the Western United States: An Ecological Approach to Nonstationarity. *Earth Future* **6**, 1097–1111 (2018).

48. Gallo, C. et al. Evaluation of CMIP6 model performances in simulating fire weather spatiotemporal variability on global and regional scales. *Geoscientific Model Dev.* **16**, 3103–3122 (2022).

49. Otón, G., Lizundia-Loiola, J., Pettinari, M. L. & Chuvieco, E. Development of a consistent global long-term burned area product (1982–2018) based on AVHRR-LTDR data. *Int J. Appl Earth Obs* **103**, 102473 (2021).

50. Lizundia-Loiola J., Otón G., Ramo R., Chuvieco E. A spatio-temporal active-fire clustering approach for global burned area mapping at 250 m from MODIS data. *Remote Sens. Environ.* **236**, 111493 (2020).

51. Giglio, L., Boschetti, L., Roy, D. P., Humber, M. L. & Justice, C. O. The Collection 6 MODIS burned area mapping algorithm and product. *Remote Sens Environ.* **217**, 72–85 (2018).

52. Harper, K. L. et al. A 29-year time series of annual 300 m resolution plant-functional-type maps for climate models. *Earth Syst. Sci. Data* **15**, 1465–1499 (2023).

53. Clelland, A. A. et al. Annual and Seasonal Patterns of Burned Area Products in Arctic-Boreal North America and Russia for 2001–2020. *Remote Sens.* **16**, 3306 (2024).

54. Hall, J. V., Argueta, F. & Giglio, L. Validation of MCD64A1 and FireCCI51 cropland burned area mapping in Ukraine. *Int J. Appl Earth Obs* **102**, 102443 (2021).

55. Hersbach et al. ERA5 monthly averaged data on single levels from 1979 to present. (ed (CDS) CCCSCSCDS). Copernicus Climate Change Service (C3S) Climate Data Store (CDS) (2019). https://doi.org/10.24381/cds.f17050d7.

56. Yuan, W. et al. Increased atmospheric vapor pressure deficit reduces global vegetation growth. *Sci. Adv.* **5**, eaax1396 (2019).

57. McElhinny, M., Beckers, J. F., Hanes, C., Flannigan, M. & Jain, P. A high-resolution reanalysis of global fire weather from 1979 to 2018 – overwintering the Drought Code. *Earth Syst. Sci. Data* **12**, 1823–1833 (2020).

58. Friedl M., Sulla-Menashe D. MODIS/Terra+Aqua Land Cover Type Yearly L3 Global 500 m SIN Grid V061. NASA EOSDIS Land Processes Distributed Active Archive Center (2022). https://doi.org/10.5067/MODIS/MCD12Q1.061.

59. Myneni R., Knyazikhin Y., Park T. MODIS/Terra Leaf Area Index/FPAR 8-Day L4 Global 500 m SIN Grid V061. NASA EOSDIS Land Processes Distributed Active Archive Center (2021). https://doi.org/10.5067/MODIS/MOD15A2H.061.

60. Running S., Zhao M. MODIS/Aqua Net Primary Production Gap-Filled Yearly L4 Global 500 m SIN Grid V061.). NASA EOSDIS Land Processes Distributed Active Archive Center (2021). https://doi.org/10.5067/MODIS/MYD17A3HGF.061.

61. Bright E., Coleman P. LandScan Global 2000. 2000 edn. Oak Ridge National Laboratory (2001). https://doi.org/10.48690/1524196.

62. Chen, J. et al. Global 1 km × 1 km gridded revised real gross domestic product and electricity consumption during 1992–2019 based on calibrated nighttime light data. *Sci. Data* **9**, 202 (2022).

63. O'Neill, B. C. et al. The Scenario Model Intercomparison Project (ScenarioMIP) for CMIP6. *Geoscientific Model Dev.* **9**, 3461–3482 (2016).

64. Wang, X., Meng, X. & Long, Y. Projecting 1 km-grid population distributions from 2020 to 2100 globally under shared socioeconomic pathways. *Sci. Data* **9**, 563 (2022).

65. Chen, G., Li, X. & Liu, X. Global land projection based on plant functional types with a 1-km resolution under socio-climatic scenarios. *Sci. Data* **9**, 125 (2022).

66. Wang, T. & Sun, F. Global gridded GDP data set consistent with the shared socioeconomic pathways. *Sci. Data* **9**, 202 (2022).

67. Abatzoglou, J. T., Williams, A. P., Boschetti, L., Zubkova, M. & Kolden, C. A. Global patterns of interannual climate-fire relationships. *Glob. Change Biol.* **24**, 5164–5175 (2018).

68. Koutsias, N. et al. On the relationships between forest fires and weather conditions in Greece from long-term national observations (1894–2010). *Int. J. Wildland Fire* **22**, 493–507 (2013).

69. Fong, Y. Fast Bootstrap Confidence Intervals for Continuous Threshold Linear Regression. *J. Computational Graph. Stat.* **28**, 466–470 (2019).

70. Chen, T., Guestrin, C. XGBoost: A Scalable Tree Boosting System. In *The 22nd ACM SIGKDD International Conference on Knowledge Discovery and Data Mining. ACM* 785–794 (2016).

71. Vega García M., Aznarte J. L. Shapley additive explanations for NO_2 forecasting. *Ecol. Inform.* **56**, 101039 (2020).

72. Zhao H., et al. Future enhanced threshold effects of wildfire drivers could increase burned areas in northern mid- and high latitudes. v2 edn. Figshare (2024). https://doi.org/10.6084/m9.figshare.28171160.

Acknowledgements

Author contributions

Hang Zhao contributed to the conceptualization, methodology, formal analysis, original draft writing, and reviewing and editing. Zhengxiang Zhang contributed to conceptualization, draft writing, reviewing, and editing. Xin Wang and Shuo Zhen contributed to the methodology and data curation. Hongyan Zhang, Zhao-Jun Bu, Jianjun Zhao, and Xiaoyi Guo contributed to the conceptualization and supervision of this work. Kejiang Wei and Long Dong contributed to data curation, resource, and manuscript revision.

Competing interests

The authors declare no competing interests.

Additional information